CONTROL SURFACE DYNAMICS AT TRANSONIC AIRSPEEDS

Holger Mai[1], Jens Nitzsche[1], Kenichi Saitoh[2] and Norio Yoshimoto[2]

[1] German Aerospace Center (DLR)
Institute of Aeroelasticity
Bunsenstraße 10, 37073 Göttingen, Germany
Holger.Mai@dlr.de
Jens.Nitzsche@dlr.de

[2] Japan Aerospace Exploration Agency (JAXA)
Aeronautical Technology Directorate
6-13-1 Osawa, Mitaka-shi, Tokyo, 181-0015, Japan
ksaitoh@chofu.jaxa.jp
yosimoto@chofu.jaxa.jp

Abstract: In a cooperative work JAXA and DLR performed two wind-tunnel experiments with a NLR7301 airfoil model performing harmonic pitch oscillations with a 25% trailing edge flap with individually controlled harmonic flap oscillations in the transonic airspeed regime. The unsteady flow field was measured with integrated pressure sensors. Nonlinear aerodynamic effects due to shock dynamics and unsteady flow separation were investigated as they are a key problem in flutter analysis of wings with control surfaces at transonic airspeeds.

For highest accuracy of the data an optical position measurement system was used to measure the motion of the model and the flap and their deformation under wind load. It turned out that the deformation under wind load cannot be neglected, but has to be taken into account when comparing the data to numerical simulations. The target therefore is to derive a simple structural model for the deformation and to get corrected data at every point of the test envelope.

1 INTRODUCTION

There is a trend that high aspect ratio wings for modern transport aircraft will become more flexible. To increase passenger comfort and to control for gust and load alleviation, new concepts for control surface design are therefore about to come. We still lack knowledge about unsteady aerodynamics for control surfaces especially in the transonic flight regime where nonlinear aerodynamic effects due to shock dynamics and unsteady flow separation may occur. The appearance of nonlinear effects due to shock dynamics and unsteady flow separation is a key problem in the flutter analysis of wings with control surfaces at transonic airspeeds. The knowledge of steady and unsteady airloads from control surface deflections or oscillations is important for gust- and maneuver load alleviation as well as for flutter prediction of aircraft. There is still a lack of wind-tunnel test results focusing on unsteady control surface aerodynamics, especially in the high transonic flow regime with strong shocks and shock induced flow separation.

Since 2007 Japan Aerospace Exploration Agency (JAXA) and German Aerospace Center (DLR) are conducting joint research on "Aeroelasticity of Flexible Aircraft and Unsteady CFD". Within the frame of this cooperation DLR and JAXA designed a wind-tunnel experiment, built a model and conducted two wind-tunnel campaigns. The main objective of this project was to define a generic experimental model in order to study the influence of unsteady movements of a wing as well as of a trailing edge control surface on the unsteady pressure field in the transonic regime. JAXA and DLR investigate the nonlinear unsteady aerodynamic behavior of wings with control surfaces in wind-tunnel tests at transonic airspeeds in order to understand the complex flow physics and to provide validation data for the improvement of numerical methods. These aim on the design of novel control surfaces, improve automatic flight control systems and increased flight envelope. Future possible applications might be an increased flight performance for fuel efficient aircraft designs, increased passenger comfort and gust load alleviation and flutter margin augmentation systems.

With increasing accuracy of numerical models it turned out that even for steady tests, the deformation of the model and the models position in the wind tunnel need to be known with an accuracy of better than 0.1%. More than that, this is valid for the unsteady motion of a model and most valid for a complex wing body and flap motion.

2 EXPERIMENTAL SET-UP

2.1 Wind tunnel facility and test set-up

The Transonic Wind Tunnel Goettingen (TWG) is operated by the foundation German-Dutch Windtunnels (DNW). The wind tunnel is a continuous run facility with a 1m x 1m adaptive test section (c.f. Fig. 1). The wind tunnel specifications are listed in Tab. 1. The ratio of the tunnel height to the chord length of the investigated airfoil model is 3.333. The top and bottom walls of the test section are adapted to the mean steady flow about the wind-tunnel model. The residual wall interference is minimized by a one-step method of wall adaptation based on a Cauchy type integral [1] using the top and bottom wall static pressure distributions. The accuracy of the wall pressures is estimated to be ±0.35% with respect to the test stagnation pressure. The displacement thickness of the turbulent wind-tunnel-wall boundary layer is predicted by Head's method [2] and is added to the wall shapes; top and bottom wall displacement thicknesses are obtained according to the measured pressure gradients at each wall while the gradient is neglected for the sidewalls [3]. The wind-tunnel walls were adapted to the steady flow at each mean incidence of the model which was chosen for the following oscillation tests.
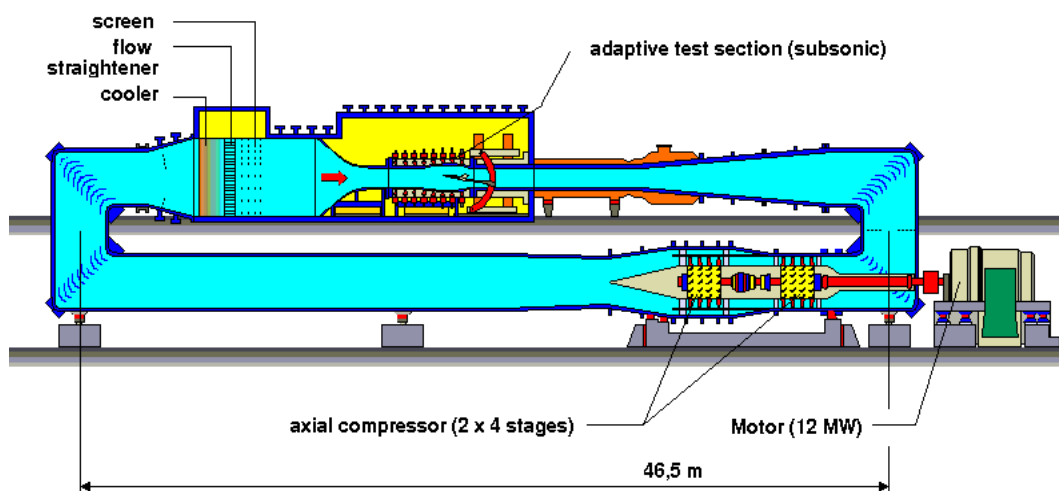

Figure 1: DNW-TWG.

Table 1: Specification of TWG.

Test section size	1.0 m×1.0 m×4.5 m
Mach number	0.3 - 0.9 (adaptive test section)
Reynolds number	0.5 Mio. – 6 Mio. (c=0.3 m)
Stagnation pressure	30 kPa – 150 kPa
Stagnation temperature	293 K – 315 K
Contraction ratio	16 : 1
Turbulence level	$\leq$ 0.10% – 0.25%
	(M0.5) (M0.8)

The model was mounted to a hydraulic pitch-oscillation test set-up which is arranged symmetrically outside of each wind-tunnel test-section side wall. Fig. 2 shows a sketch of this pitch-oscillation test set-up with the model installed. The angle of attack of the symmetrically installed model can be varied by ±20° via two hydraulic exciters (Tab. 2) operated in phase opposition. Forced pitching oscillations up to a frequency of 120 Hz are possible. The suspension system comprises a compensator, a bearing, a piezoelectric balance and a bar acting as a reference for laser triangulators. By these the instantaneous angle of attack can be measured by triangulation.
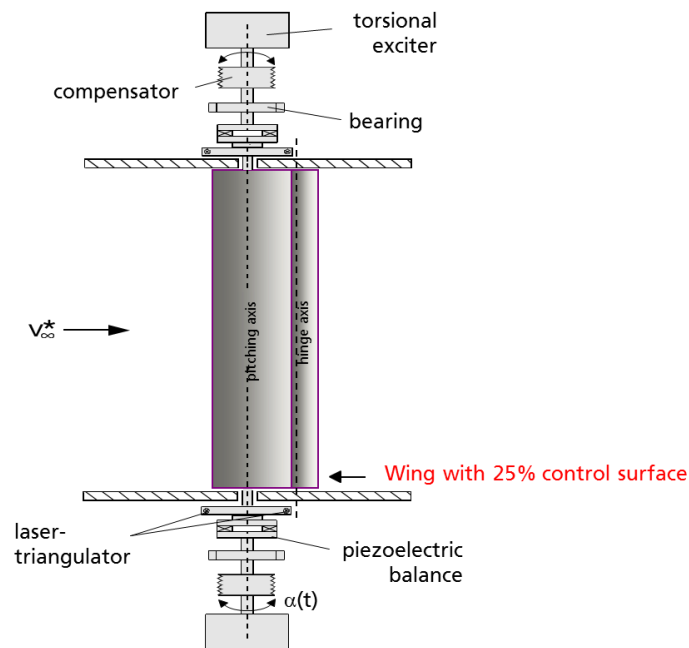

Figure 2: Pitch oscillation set-up.

Table 2: Specification of the hydraulic actuator for pitch motion.

Max. torque	200 Nm
Max. frequency	120 Hz ($\leq$ 50 Hz in typical)
Max. amplitude	10° ($\leq$ 10 Hz)
Typical amplitude	±1° (at 50 Hz)
Max. moment of inertia of model	0.1 kgm^2

3

2.2 Model

For the test a new wind-tunnel model was built. The wind-tunnel model was designed to perform pitch oscillations and independent pitching oscillations of a control surface simultaneously. Both degrees of freedom are excited by hydraulic pitching actuators. A NLR7301 [4] airfoil was chosen and the model was built from CFRP. The span is 998 mm, the cord length c = 300 mm. The model encompasses a trailing-edge flap of 25% chord length over the full span which was hydraulically driven by two miniature hydraulic actuators mounted on the bars outside of the wind-tunnel walls. The actuators worked synchronized but in phase opposition to move the control surface by a maximum amplitude of $\Delta\alpha = 10°$. With reduced amplitude oscillations of the control surface up to a frequency of 70 Hz were possible.

The flap hinge line position is at 75% of the chord. For the stress analysis a designed air flow condition of Ma = 0.800 and a wind tunnel total pressure of 150 kPa at a stagnation temperature of 310 K was chosen. A safety factor of 1.5 was achieved. The lowest natural eigenfrequency was desired to be above the highest excitation frequency of 50 Hz.

Table 3: Design operational range.

Max. Mach	0.8
Max. AOA	3°
Max lift c_l	0.959
	(designed aerodynamic loads were calculated with Euler)
total pressure p_0	150 kPa
dynamic pressure q	44 kPa
Lift force	1298 kg
lift of the flap:	LH=353→300 kg
	(reduced from analytical value of 353 kg)
hinge moment of the flap:	MH=600 kgcm
	(reduced from analytical value of 819 kgcm)
Max. pitching motion	45 Hz, $\Delta\alpha = 2°$
Max. flap motion	50 Hz, $\Delta\alpha = 2°$

Based on the result for the inertial forces the maximum model mass was 14 kg and 0.1 kgm^2 or less, respectively.

The model was equipped with 54 differential unsteady pressure transducers of which 44 were arranged in one row in the mid-span section and 10 of them were also placed on the upper and lower surfaces immediately upstream of the hinges (see Fig. 3). Several sensors were placed on the control surface. The so-called pressure-based lift, pitching-moment and drag coefficients could be integrated from the measured airfoil surface pressures. Besides the pressure sensors, the model was equipped with strain gauges to monitor the model loads. Global lift force and pitching moment are in addition measured by the piezoelectric balance. Tab. 4 lists all sensors installed in the model.

Figure 3: Position of orifices for pressure sensors.

Table 4: Sensors installed in the model.

Pressure transducer	Kulite XCQ-107-093-5D
Strain gage	Kyowa KFG-02-120-C1-11L3M2R
Hall sonsors	Honeywell HMC1501
	Honeywell SS496A1
Potentiometer	Midori-sokki CPP-35B-45

The model was mounted to the test rig via the adjustment bar. On the adjustment bar there were miniature hydraulic actuators installed that drive the flap, one actuator on each side. Tab. 5 shows the specifications of these actuators. By that, pitching motion of the whole model and pitching of the control surface could be excited simultaneously and independently from each other. A test was conducted (cf. Fig. 4) to check how the hydraulic actuator on the bar behaves in a vibrating (model global pitch) environment. The actuator was shaken with an acceleration of up to 10 G and no problem was found in the control surface drive.
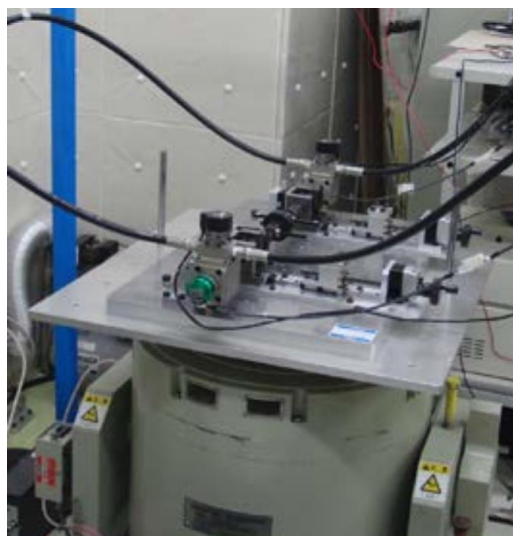

Figure 4: Vibration test of hydraulic flap pitch actuator.

Table 5: Specification of hydraulic actuators for flap.

Hydraulic pressure	18 MPa
Drive angle	20°
Max. static torque	60 Nm
Max. angular velocity	628°/s (@ ±2°, 50 Hz)
Weight	≤ 1300 g
Tolerance to vibration	16.9 G (15 G for potentiometer)

The flap angle could be measured by Hall sensors that were installed at the hinge axes. The sensor is attached to the main wing body near the hinge, and a neodymium permanent magnet was glued to the control surface. The output data of the Hall sensor calibration test is shown in Fig. 5.
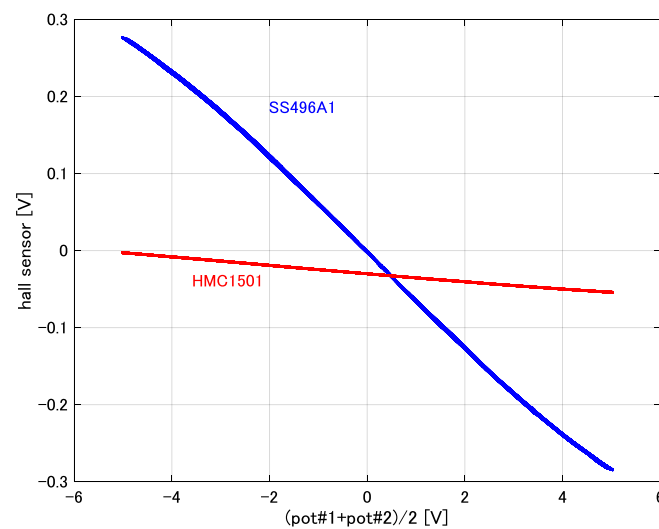
Figure 5: Output of Hall sensor calibration test.

To measure its center of gravity, the model was placed with its axis on straight edges. By putting additional weights on the bar, the model could be balanced and the center of gravity shifted into the axes of rotation.

A transition strip was placed on the models upper surface at 7% chord to force turbulent boundary layer transition. Transition dots of 0.1016 mm height were used. On the lower side a transition strip of the same height was placed at 14% chord. The effectiveness was checked with an infrared camera at the time of the wind-tunnel test.

2.3 Additional measurement techniques:

The global motion of the model and the flap and local model deformations were measured with the optical marker based photogrammetric system PicColor from F.I.B.U.S. Research Institute.
PicColor records the movements of defined markers in three-dimensional space. Based on the correlation of two camera systems, x-, y- and z-coordinates of markers in a calibrated volume can be restored with very high frequency depending on the frame rate of the cameras, the number of markers and the computing power of the data analyzing system. In the present system frequencies of up to 1 kHz are possible for a number of markers of up to 100. The

6

evaluated position results are stored to disc for later evaluation or sent to another computer via TCP/IP and can be visualized as time series. Markers are circular flat areas on the surface (paint) that have the greatest possible contrast to the background. PicColor divides the images transmitted by the cameras into 256 grayscales. The value zero stands for black and the value 255 for white. The markers can be recognized by the PicColor software from a contrast difference of approx. 40.

The images are recorded by two cameras which observe the same image space from different positions (Fig. 6). The positions of the individual markers can only be determined in the individual images of the cameras in two coordinates. In order to obtain the positions of the markers in three-dimensional space, a calibration must be carried out. In general, a calibration frame is used for this, on which light bulbs are plugged that are switched on one after the other. The light bulbs have a spherical glass bulb so that a circular marker can be detected from any view angle. For an optimal calibration at least 12 markers are necessary, which span the space of the later measuring range. The positions of these markers with respect to a common coordinate origin are written to a text file which is read by the PicColor software during calibration. At each image acquisition only one marker may be recognized in order to enable a clear assignment to the coordinates stored in the text file. If several markers are recognized in an image or if certain exclusion criteria are fulfilled, this image is discarded. For the calibration, it is therefore necessary to create a dark environment in which no reflections of the light bulbs can occur. If the calibration is successful, PicColor calculates a transformation matrix for each camera with which it can now map the 2D positions of the markers in a 3D coordinate system. After calibration, the cameras must not be adjusted either in their position or in their inclination.
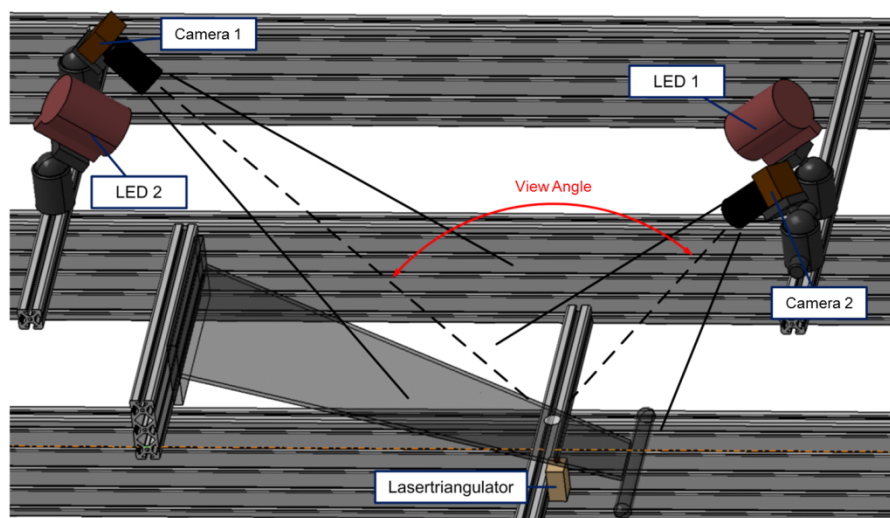

Figure 6: Principle of PicColor test set-up.

In order to be able to perform a measurement, the model is placed in the observation space of the cameras and the markers are defined within the software. Since PicColor evaluates in real time, only sections within the recorded images can be processed in order to keep the computing effort as low as possible. These sections, also called ROIs (Regions Of Interest), are automatically set around each defined marker. The size of the ROI can be adjusted according to the requirements. If you observe a few markers traveling a large distance within an image progress, it is recommended to set a large ROI. If you evaluate several markers close to each other, you have to select a ROI so small that only one marker within one ROI can be detected. Due to the computation-intensive real-time evaluation of the PicColor software, only a limited number of markers can be defined. With the hardware components

used in the PicColor measuring computer, up to 100 markers can be evaluated with a maximum frame rate of 1000 fps.

2.4 Data acquisition system

All analogue signals were recorded with a Dewetron data acquisition system. This encompasses a DEWE-818 host computer and a DEWE-51-PCI frontend with 128 analogue input channels. Delta-Sigma A/D converters with 24 bit bandwidth and up to 204.8 kHz sampling rate per channel convert the analogue signals to digital. Several frontends can be connected to increase the number of channels. All channels are fully synchronized.

Wind-tunnel data like Mach number, dynamic pressure and wall pressures are measured by the wind-tunnel data system and transferred to the Dewetron system as a text file.

There is no differentiation between steady (no model or flap motion) and unsteady (model pitch or flap motion). For all data points time series of the signals are recorded. For steady data points 20480 samples at a sampling rate of 1200 Hz are recorded. For unsteady data points the sampling rate is set to 128 Hz times the excitation frequency. So, for a flap oscillation frequency of 25 Hz the sampling frequency is set to 3200 Hz. By that, phase synchronous averaging is very simple.

3 TEST PRE- AND POST PREPARATION

3.1 Wind tunnel vibration test

A ground vibration tests was conducted with the model installed in the wind tunnel. Tab. 5 shows the parameters for the first 8 eigenmodes. Fig. 7 shows the main mode shapes. The lowest eigenfrequency was at the first pitch rotation mode at 70.7 Hz. The first bending was seen at 109.5 Hz. By that, the design criteria were met at the lowest level.

Model safety was confirmed by flutter analysis based on the structural model and the transonic doublet lattice method (TDLM).

Table 5: Eigenmodes of W/T model.

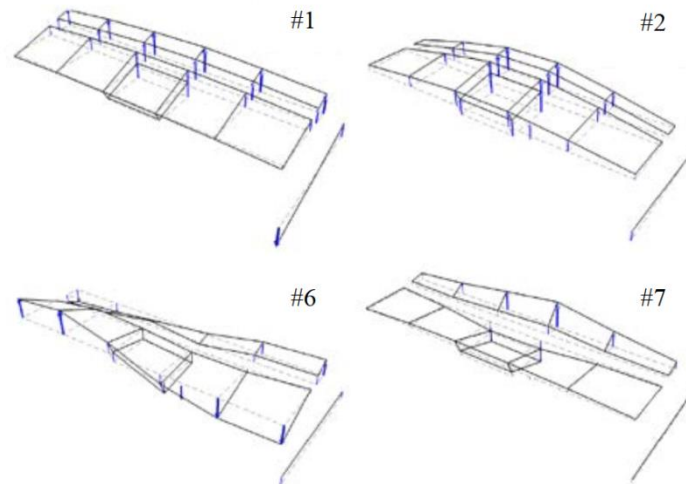| Mode #	Frequency [Hz]	Damping [%]	Modal mass [kgm2]	Mode
1	70.7	2.28	5.7822	pitch
2	109.5	1.96	2.2484	bending 1
3	169.1	1.98	1.6627	pitch & torsion
4	209.5	2.51	4.3185	bend & heave
5	291.3	2.53	18.3873	pitch & bend.2
6	352.8	3.66	1.7469	torsion
7	441.0	1.35	0.8842	flap rotation
8	460.8	2.39	1.5297	flap rotation & bend.2

Figure 7: Mode shapes of W/T model.

3.2 Shape measurement

After the wind tunnel test a three-dimensional measurement of the surface was performed at "Carl Zeiss Industrielle Messtechnik GmbH" in Peine/Germany to confirm the models shape. The model is in the wing design data at the time of production and was manufactured with an accuracy of ± 0.25 mm which was confirmed by the measurement.

Figure 8: Result of surface scan.

3.3 Dynamic calibration test

A dynamic calibration test of the unsteady pressure sensors was conducted (Fig. 9). By a 60 W output horn (University sound model-ID60C8) pressure fluctuations were given to the orifice in the models surface (Fig. 9 red tube). Just above the pressure hole a reference pressure was measured by an identical pressure sensor. By that response data a transfer function could be calculated and a possible correction in gain and phase depending on the frequency could be derived. For a pressure sensor installed directly under the models surface with minimal volume above the sensors membrane we see nearly no change in gain and

phase. But some sensors had to be installed with a metal pipe. There some delay in gain and phase can be seen (Fig. 10).
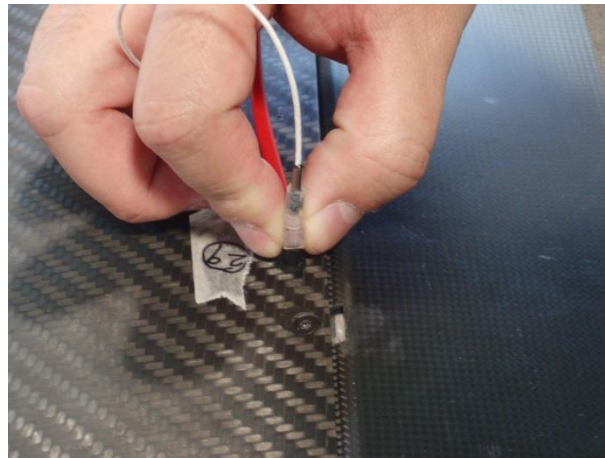
Figure 9: Measurement of the transfer function for pressure sensors.
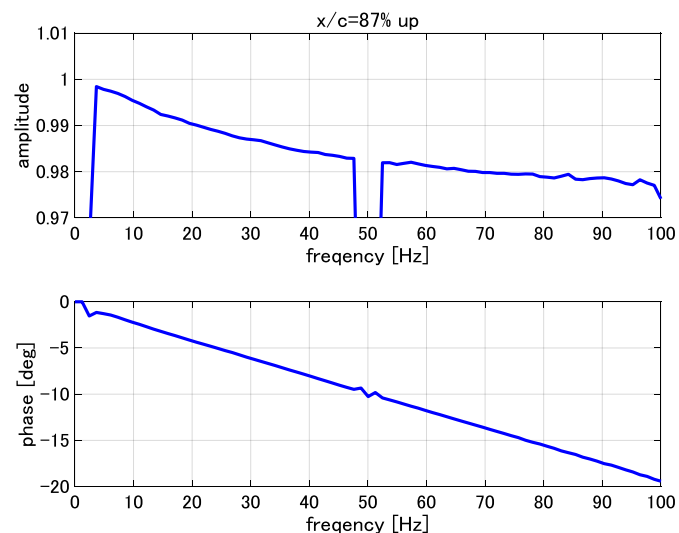
Figure 10: Transfer function for pressure sensor on the flaps upper side at x/c=87%.

4 TEST CONDUCTION

4.1 Test program

The main focus of the test program was on the unsteady measurements in the transonic region. But as a reference also a complete steady test program and data points at subsonic conditions was taken.

For all test conditions the Reynolds number was fixed at about 2 mio. This was realized by adjusting the total pressure in the wind-tunnel. The wind-tunnel can be evacuated and pressurized between 30 and 140 kPa.

Steady test points were taken at the following conditions:

$Ma \in \{0.500, 0.660, 0.680, 0.700, 0.720, 0.740, 0.750, 0.760, 0.770, 0.780\}$
$\alpha_0 \in \{-0.6° : +5.0°\}$
$\delta_0 \in \{-5° : +5°\}$

10

Unsteady test points were taken at the following conditions:

$Ma \in \{0.500, 0.700, 0.720, 0.740, 0.750, 0.760, 0.770, 0.780\}$
$\alpha_0 \in \{0.0°, 0.6°, 1.4°, 1,6°, 1.8°, 2.4°, 3.4°, 4.0°\}$, $\Delta\alpha = 0.2°$
$\delta_0 = 0.0°$, $\Delta\delta \in \{0.2° : 5.0°\}$

4.2 Test execution

The sequence of test execution was as follows: First the total pressure in the wind tunnel was set according to the desired Mach number to meet the Reynolds number. Then the Mach number was set to its target value. Then the mean steady angle of attack and the mean steady flap angle were set to their target values. After that, the top and bottom wind-tunnel walls were adapted. Fig. 11 shows the shape of the adaptive wall for a test condition at Ma = 0.740. Finally a steady data point was taken or the model or flap set to its oscillation and a data point taken.
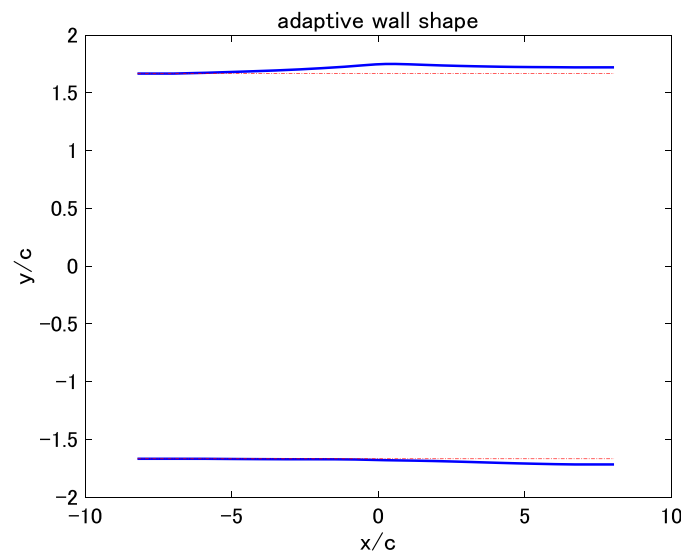
Figure 11: Shape of the adaptive wall.

4.3 Model and flap motion

Examples of the results are shown in Fig. 12 and Fig. 13. Airflow condition is Mach 0.74 and wind tunnel total pressure $p_0 = 50$ kPa. The model is set to a mean angle of attack of $\alpha_0 = 1.2°$, the flap angle is set to $\beta_0 = 0°$. The flap is set to a harmonic pitching motion with an amplitude of $\Delta\beta = 1.2°$ at a frequency of $f = 30$ Hz. In Fig. 12 the instantaneous pressure distributions for 128 time steps over one full oscillation period are plotted. Suction (upper) side is blue, pressure (lower) side is red. A distinct shock far upstream of the hinge line can be seen. The shock shows a high dynamics and moves over 15% of the chord. For the same test condition Fig. 13 presents pressure signals of three selected pressure sensors on the upper side of the model around the shock location. Pressure sensor no. 24 is located at 35% of the chord. At that position it is swept over only temporary during the oscillation period of the flap and some fluctuations occur. Sensor no. 25 at 40% seems to experience no fluctuations during the oscillation and sensor no. 26 at 45% is in an area of large fluctuations under or shortly behind the shock.
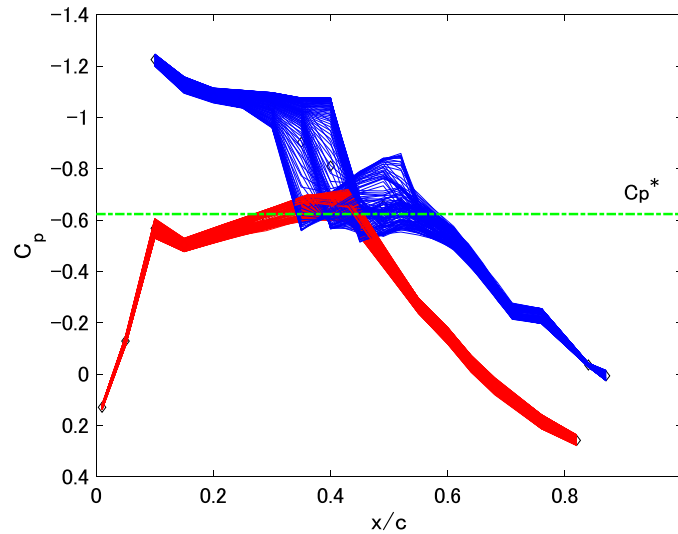
11

Figure 12: Pressure distribution at $\alpha = 1.2°$ and flap oscillation with 30 Hz, $\Delta\beta = 1.2°$, $\beta_0 = 0°$.
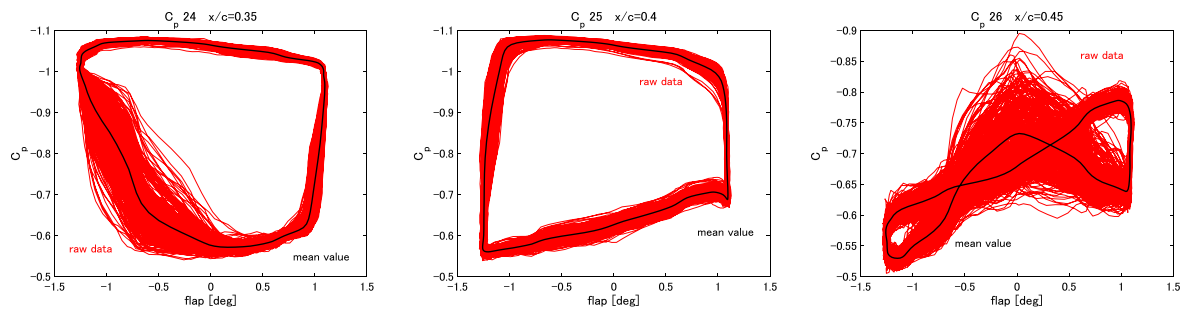

Figure 13: Time series for the pressure sensors 24-26.

5 ANALYSIS OF RESULTS

5.1 Global steady lift and moment polars

The global lift coefficients based on pressure and balance measurements are presented in Fig. 14. It can be noted that the values integrated from the pressure measurements are slightly higher than that from the piezoelectric balance. The reasons for that are 3D effects in the flow over the airfoil: the pressure sensors measure the lift in the center section of the airfoil model. Due to wall effects, the lift decreases at the side walls of the test section but the integration assumes 2D flow. In contrast to that, the balance measures the total lift distributed over the airfoil model. That is, due to the 3D effects, slightly lower.

For comparison results from [5] for a NLR7301 airfoil model are plotted in the same graph. It can be observed that for the moderate transonic case at Ma = 0.702 the agreement is quite good. For the strong transonic case at Ma = 0.743 a difference in lift coefficient is present of nearly 0.2. Obviously the 3D effects are more pronounced in the presence of strong shocks. Also, the finite stiffness of the model and probably especially the finite stiffness of the flap are causing a de-cambering of the model and by that a decrease in lift coefficient.
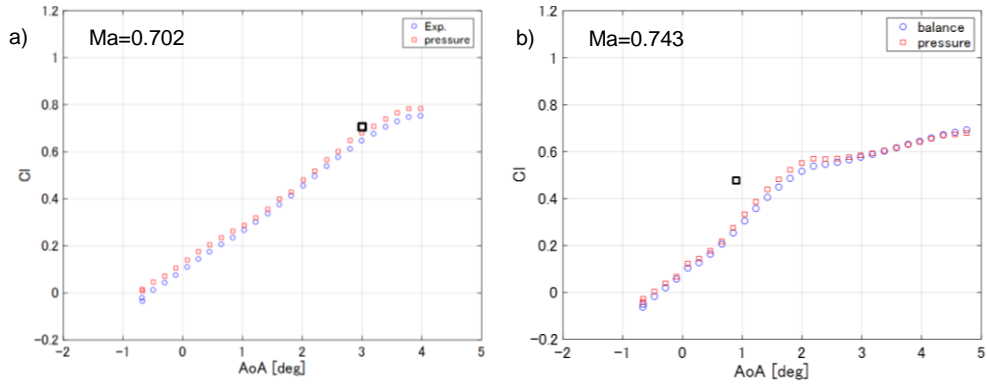
12

Figure 14: Global lift coefficient polars for Ma=0.702 (a) and Ma=0.743 (b).
Black squares are comparison data from [5]: a) Run 14405: Ma=0.696, α_0=3°, Re=2.1mio.
b) Run 16908: Ma=0.744, α_0=0.85°, Re=2.2mio.

5.2 Results with oscillating flap

5.2.1 Amplitude variations

Amplitude variations with oscillations of the flap of up to 5° (10° peak-to-peak) are shown in Fig. 15. The conditions represent attached flow (Ma = 0.74, α_0 = 0.6°). A slight decrease in the magnitude with increasing amplitude can be observed. The phase stays constant over the whole range of amplitudes. Plotted in red and blue are the mean lift coefficients for the steady flap angles (flap polar).
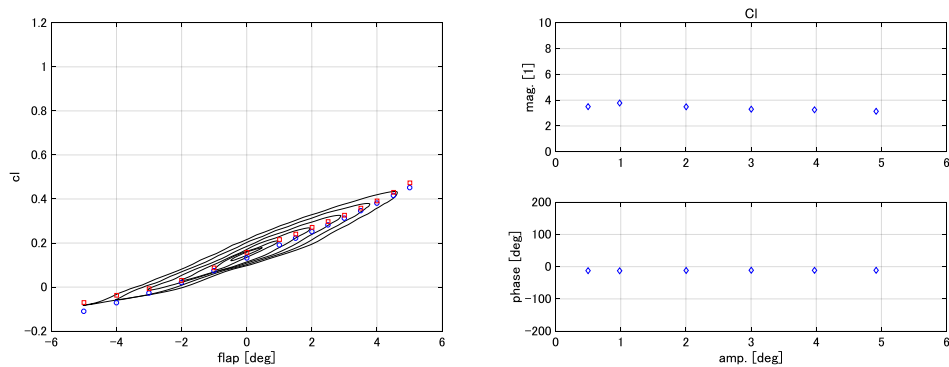
Figure 15: Global lift coefficient vs. flap angle (left). Results of transferfunction (right). Ma = 0.74, α_0 = 0.6°).

Fig. 16 shows amplitude variations of the flap with the same oscillations as in Fig. 15 for separated flow conditions (Ma = 0.74, α_0 = 2.4°). Distinct nonlinearities can be observed over the whole range of amplitudes.

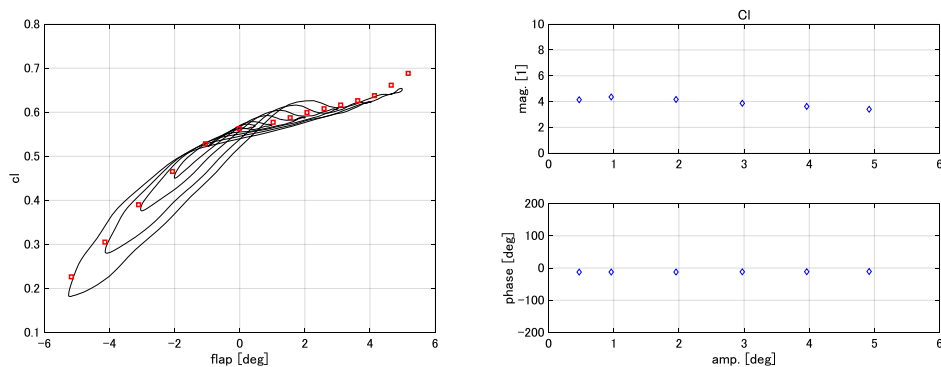Figure 16: Flap amplitude variations in separated flow conditions (Ma = 0.74, α_0 = 2.4°).

13

5.2.2 Frequency variation of flap motion

Fig. 17 and 18 show the unsteady lift coefficient excited by the flap motion. The amplitude of the flap excitation was 0.2° in all cases. In the attached flow case the magnitudes of the lift coefficient response decrease as the excitation frequencies increase (Fig. 17, right). The trend follows Theodorson theory, although the values are systematically below. In the separated flow case the magnitude shows a distinct peak around 45 Hz. It could be caused by the resonance of a buffet frequency.
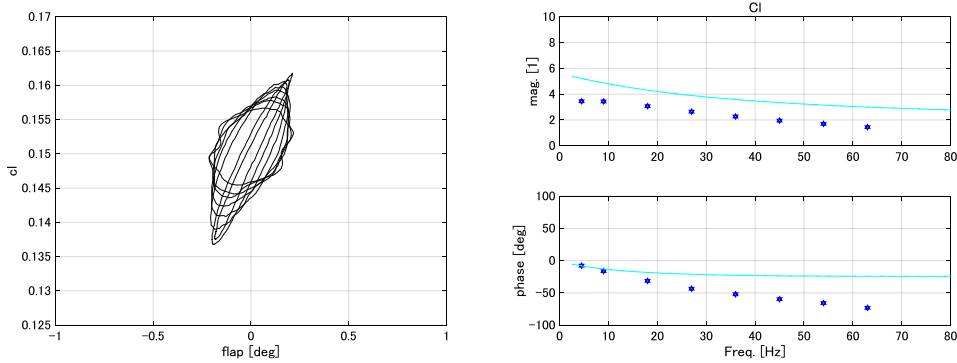
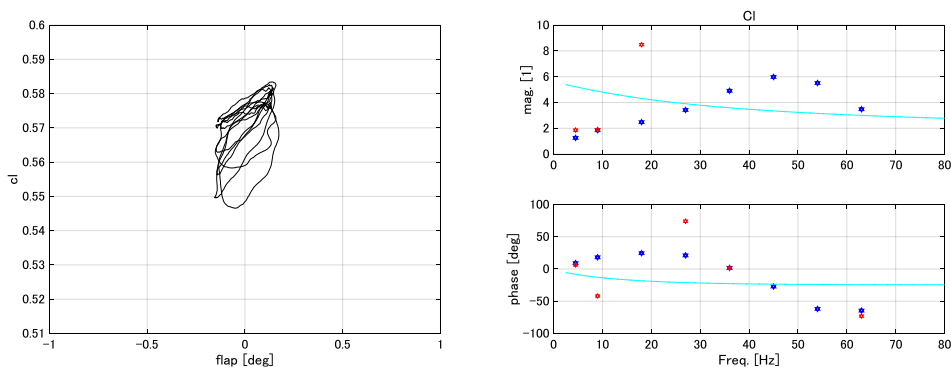Figure 17: Flap frequency variations in attached flow (Ma = 0.74, $\alpha_0 = 0.6°$)

Figure 18: Flap frequency variations in separated flow (Ma = 0.74, $\alpha_0 = 2.4°$)

5.3 Behavior of the flap

For a validation of high accuracy we need to take into account even small deviations of the model contour, its angle of attack and the flap angle. For that we further investigate the dynamic behavior of the flap. The target is to derive a correction methodology to get corrected values or all data points for validation.

Based on the PicColor data for each steady condition an actual in-situ flap angle was calculated and compared with the set value. Fig. 19 shows the measured flap angle vs. the nominal set value for a polar at Ma = 0.74. From both values a flap correction value was calculated as the difference of the nominal flap angle and the PicColor flap angle.
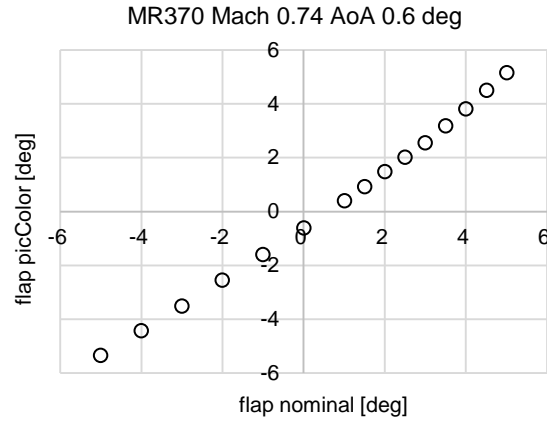
Figure 19: Flap angle measured by PicColor compared with nominal flap angle.

Second a hinge moment was reconstructed based on the pressures measured by the sensors on the flap. As there was no pressure sensor in the trailing edge, the pressure at the trailing edge Cpte was calculated as the weighted mean of the extrapolated pressure on the upper side of the flap Cpteup and the extrapolated pressure on the lower side of the flap Cptelo (Fig. 20). The pressure on the upper side was extrapolated from the last two pressure sensors Cp[0] and Cp[1] to the position of the trailing edge xte to get an upper side trailing edge pressure Cpteup. Then the pressure on the lower side was extrapolated from the last two sensors Cp[n-1] and Cp[n] to the trailing edge to get an lower side trailing edge pressure Cptelo.

$$\text{Cptelo } = Cp[0] + (xte - x[0]) * (Cp[1] - Cp[0]) / (x[1] - x[0]) \tag{1}$$
$$\text{Cpteup} = Cp[n-1] + (xte - x[n-1]) * (Cp[n-2] - Cp[n-1]) / (x[n-2] - x[n-1]) \tag{2}$$

Then we calculate weighting factors wfup and wflo for the two pressures depending on the distance to the trailing xte edge of the last upper and lower sensor.

$$\text{wfup } = (xte - x[0]) / (xte - x[n-1] + xte - x[0]) \tag{3}$$
$$\text{wflo } = (xte - x[n-1]) / (xte - x[n-1] + xte - x[0]) \tag{4}$$

Then we calculate the weighted mean of the two trailing edge pressures:

$$\text{Cpte} = wfup * Cpteup + wflo * Cptelo \tag{5}$$

For the upper and lower pressure at the leading edge of the flap we used the weighted mean pressure value of the last sensor on the models main body and the first sensor on the flap on the upper and lower side. By this we get the best possible value for the hinge moment.
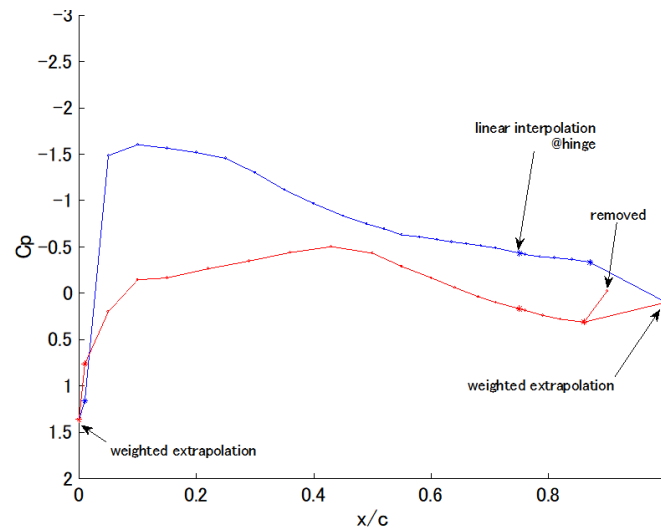
15

Figure 20: Treatment of "missing" sensors for integration of lift from pressure sensors.

The dependency of the flap correction angle (flap deformation) on the hinge moment is depicted in Fig. 21. Two regions can be clearly identified: The region of attached flow and the region of separated flow: for the linear region of attached flow we add the constraint that the deflection correction has to be zero for zero hinge moment. From that we can derive a linear correction function for the flap.
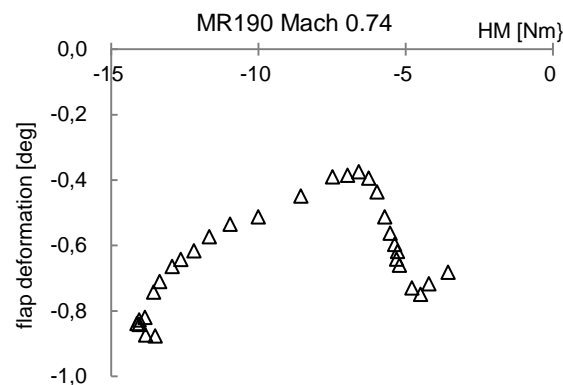

Figure 21: Flap correction value against hinge moment.

It is obvious that there is no simple elastic model that can explain the complex deflection behavior of the model.

Probably this has to be attributed to a more complex flow situation. The aspect ratio of the model is too small to neglect the side-wall interference effects. Corner separation may interfere with the assumed perfect 2D flow.

This can already be seen in the difference between the integrated lift values from the mid-span pressure sensors and the balance results that integrate over the full span of the model.

6 SUMMARY

Measurements of unsteady aerodynamics in a cooperative wind-tunnel experiment by DLR and JAXA with a two-dimensional model with NLR7301 airfoil shape have been performed. The model comprises a 25% chord trailing edge control surface that could be actuated individually from the model with an integrated hydraulics.

A comprehensive data base, including steady configurations and unsteady global pitch and flap oscillations at several excitation amplitudes and frequencies was created for CFD code validation. It turns out that for an increased data quality the elastic deformation under wind load must be taken into account and data has to be corrected. Due to the nonlinear loading on the airfoil model and the flap a simple correction model over the whole range of parameters does not seem feasible. Therefore further investigation on the structural behavior of the model and the flap are scheduled. Also 3D effects and wall interference in the wind tunnel affect the nominal 2D measurement results.

7 REFERENCES

[1] Wedemeyer, E., Taylor, N. J., and Holst, H., "Adaptive Wall Techniques", AG 336, AGARD, 1998.

[2] Cebeci, T., and Bradshaw, P., "Momentum Transfer in Boundary Layer", Washington, D.C., Hemisphere Publishing Corp.; New York, McGraw-Hill Book Co., 1977. 407 p., Vol. -1, 1977.

[3] Jacobs, M., "Treatment of the Wall Boundary Layer in the Wall Adaptation Procedure and Steady Wall Adaptation for Dynamic Tests", private communication, DNW BU GuK, Goettingen, 2002.

[4] Tijdeman, H., and Seebass, R., "Transonic flow past oscillating airfoils", Annual Review of Fluid Mechanics, Vol. 12, 1980, pp. 181–222.

[5] Zwaan, R. J., "NLR7301 supercritical airfoil. Oscillatory pitching and oscillating flap" in AGARD Report No. 702 "Compendium of unsteady aerodynamic measurements", ISBN92-835-1430-0, 1982

COPYRIGHT STATEMENT